How to cite: *Angew. Chem. Int. Ed.* **2023,** *62,* e202300110
doi.org/10.1002/anie.202300110

Semihydrogenation

Molecule Saturation Boosts Acetylene Semihydrogenation Activity and Selectivity on a Core-Shell Ruthenium@Palladium Catalyst

Chuwei Zhu[+], Wenlong Xu[+], Fang Liu, Jie Luo, Junling Lu, and Wei-Xue Li**

Abstract: Increasing selectivity without the expense of activity is desired but challenging in heterogeneous catalysis. By revealing the molecule saturation and adsorption sensitivity on overlayer thickness, strain, and coordination of Pd-based catalysts from first-principles calculations, we designed a stable Pd monolayer (ML) catalyst on a Ru terrace to boost both activity and selectivity of acetylene semihydrogenation. The least saturated molecule is most sensitive to the change in catalyst electronic and geometric properties. By simultaneously compressing the Pd ML and exposing the high coordination sites, the adsorption of more saturated ethylene is considerably weakened to facilitate the desorption for high selectivity. The even stronger weakening to the least saturated acetylene drives its hydrogenation such that it is more exothermic, thereby boosting the activity. Tailoring the molecule saturation and its sensitivity to structure and composition provides a tool for rational design of efficient catalysts.

Introduction

Success of supported transition metal catalysts in heterogeneous catalysis depends ultimately on whether and how high activity and selectivity are simultaneously achieved and remain stable under operando conditions. Guided by the Sabatier principle and Brønsted–Evans–Polanyi relationship, optimum catalysts with high activity should interact neither too strongly nor too weakly with reactants from a catalytic cycle point of view.[1] However, the selectivity often declines with activity improvements, due to the constraints of the scaling relations of adsorption between reactants and products on given catalysts.[2] Catalysts with high dispersion such as small nanoparticles (NPs), clusters, and single-atom catalysts (SACs) suffer, in addition, from poor stability due to a high ratio of low coordination sites (LCSs) exposed.[3] Increase of the selectivity and stability without expense of the activity, and vice versa, remains a challenge and requires more systematic investigation, as addressed in this work.

Semihydrogenation of acetylene plays a vital role in the chemical industry for purifying ethylene feeds in polyethylene production by removing trace amounts of acetylene impurity from steam cracking.[4] Selective and rapid conversion of acetylene in excess of ethylene and prohibition of overhydrogenation to ethane are crucial to minimize site blockage and poisoning of the downstream catalysts, and highly selective catalysts at high conversion are essential but difficult to achieve. Among others, Pd catalysts have received great attention owing to their high activity, but the low selectivity to ethylene and rapid deactivation due to formation of coke and green oil limit their applications.[5] Alternatively, mixing Pd with less reactive metals to form bimetallic alloys or ordered intermetallic compounds has been extensively studied[6] where continuous Pd ensembles are broken and/or surrounded by less reactive metals. The electronic and geometric properties of the Pd species are changed in such a way to weaken the ethylene adsorption for a higher selectivity but generally at the cost of activity. SACs often exhibit a high selectivity in various reactions including semihydrogenation of acetylene.[7] However, a higher temperature was required for its lower activity, and the limited number of active sites available and lifetime remain open questions.[3a,b,8]

Bimetallic core–shell catalysts provide a different strategy to control the electronic and geometric properties of catalysts owing to their unique strain and ligand effects, yet without loss of the continuous and abundant metal ensembles exposed.[9] For high activity, the metal overlayers in expansion with an upshift of the d-band center were widely explored. For instance, the Au@Pt core–shell catalysts were found to improve the hydrogenation activity of *p*-chloronitrobenzene by an increase of the binding strength while retaining high selectivity to haloanilines.[2c] The Au@Pd catalysts were reported to be highly active for hydrogenation of 1,3-butadiene along with a high selectivity.[10] However, for semihydrogenation of acetylene, increase of the binding would inhibit ethylene desorption and lower the selectivity. On the other hand, the metal overlayers in compression

[*] Dr. C. Zhu,[+] Dr. J. Luo
Hefei National Research Center for Physical Science at the Microscale, University of Science and Technology of China
Hefei, Anhui 230026 (China)
W. Xu,[+] F. Liu, Prof. J. Lu, Prof. W.-X. Li
Key Laboratory of Precision and Intelligent Chemistry, School of Chemistry and Material Science, Collaborative Innovation Center of Chemistry for Energy Materials (iChEM), University of Science and Technology of China
Hefei, Anhui 230026 (China)
E-mail: junling@ustc.edu.cn
wxli70@ustc.edu.cn
Prof. W.-X. Li
Hefei National Laboratory, University of Science and Technology of China
Hefei, Anhui 230088 (China)
[+] These authors contributed equally to this work.

along with downshift of the d-band centers could weaken the ethylene adsorption for a higher selectivity, but the activity might be lowered. Moreover, activity and selectivity of the exposed overlayers depend sensitively on the ligand effects from the core and distribution of the high coordination sites (HCSs) and LCSs, which are both a complex function of the layer thickness and core size.

We resort here to molecule saturation and its sensitivity on the change in catalyst geometric and electronic properties to resolve the dilemma between activity and selectivity of semihydrogenation of acetylene. Specifically, based on comprehensive first-principles calculations, we disclose that though there are similar qualitative trends for adsorption of reactants, products, and intermediates involved in the strain, overlayer thickness, and HCSs/LCSs of Pd-based, their different saturations lead to distinct structure sensitivity, where the least saturated molecule is most structurally sensitive. By utilizing the distinct structure sensitivities of acetylene and ethylene, we found that the Ru terrace supported Pd ML in compressive strain, which is stable under the reaction conditions, promotes both acetylene hydrogenation and ethylene desorption and simultaneously boosts activity and selectivity. Guided by theory, the monometallic Pd nanocatalysts with different diameters and large size Ru@Pd core–shell catalysts with various shell thickness using advanced atomic layer deposition (ALD) were synthesized and applied in semihydrogenation of acetylene. The Ru@Pd core–shell catalyst with a ML thickness of Pd exhibits high activity and selectivity at the same time, superior to the core–shell catalysts with thicker shell and monometallic Pd nanocatalysts, regardless of the size, and in excellent agreement with theory.

Results and Discussion

Adsorption of acetylene, ethylene, and ethane with increase of the saturation on Pd(111), Pd(211), and Pd_{55} (Figure S1)[2b,c,11] were first investigated and the most favorable adsorption sites at the low coverage (details in the Supporting Information) were identified. Considering typical reaction conditions, $T=333$ K, $P(C_2H_2)=0.01$ atm, $P(C_2H_4)=0.5$ atm, $P(C_2H_6)=0.002$ atm, $P(H_2)=0.02$ atm, corresponding free energies of adsorption G_{ads} were calculated and plotted in Figure 1a and Table S1 with the geometries presented in Figure 1b. Regardless of the surfaces considered, C_2H_2 exhibits the strongest binding and most exothermic G_{ads} from -2.28 to -1.75 eV, whereas C_2H_4 has a considerably weaker binding with G_{ads} from -0.93 to -0.78 eV, and C_2H_6 becomes even endothermic from $+0.19$ to $+0.34$ eV. As expected, the adsorption is structurally sensitive and the adsorption at LCSs binds the molecules

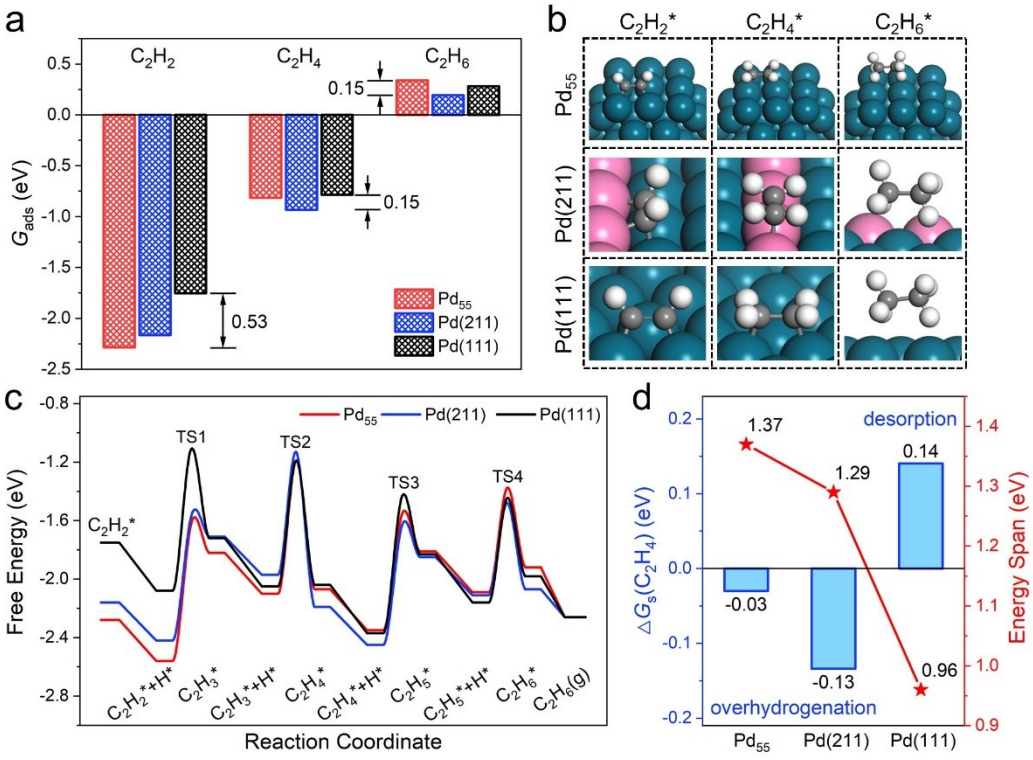

Figure 1. Structural sensitivity for semihydrogenation of acetylene on Pd(111), Pd(211), and Pd_{55}. a) Free energies of adsorption. b) Optimized configurations of C_2H_2, C_2H_4, and C_2H_6 (cyan = Pd, pink = stepped Pd, gray = C, white = H). c) Gibbs free energy profiles of hydrogenation for C_2H_2 molecular adsorption and $2H_2$ molecular dissociative adsorption. d) Calculated $\Delta G_s(C_2H_4)=G_{act}-|G_{ads}|$ for C_2H_4 selectivity (blue) and energy span (red) for C_2H_2 hydrogenation to C_2H_4. Reaction conditions: $T=333$ K, $P(C_2H_2)=0.01$ atm, $P(C_2H_4)=0.5$ atm, $P(C_2H_6)=0.002$ atm, $P(H_2)$ - =0.02 atm.

stronger than those at HCSs. Importantly, the structure sensitivity is molecule dependent, the least saturated C_2H_2 not only has the strongest binding strength but also exhibits the greatest dependence in calculated G_{ads} varying by 0.53 eV. Whereas on increasing the adsorbate saturation to C_2H_4 and C_2H_6, not only the binding strengths decrease gradually but the corresponding dependence becomes modest too, varying by 0.15 eV only. As explained below, along with a gradual increase of saturation of the C_2H_x ($x=2,3,4,5$, and 6) intermediates involved in hydrogenation, their different binding strengths and structure sensitivities are decisive to the overall activity and selectivity.

Figure 1c shows the calculated Gibbs free energy profiles of hydrogenation via the Horiuti-Polanyi mechanism[12] on Pd(111), Pd(211), and octahedron Pd_{55}, along with transition states (TSs), barriers, and energetics in Figures S2 and S3, and Table S2. The first hydrogenation of C_2H_2 to C_2H_3 on Pd(111) is endothermic with a ΔG of 0.36 eV and a hydrogenation barrier of 0.96 eV. For Pd(211) and Pd_{55}, the corresponding ΔG become significantly more endothermic by 0.71 and 0.74 eV, though the changes in barriers of 0.83 and 0.92 eV are modest. This is mainly because Pd(211) and Pd_{55} with LCSs stabilize the least saturated C_2H_2 more than the hydrogenated form, as detailed above. For the second hydrogenation from C_2H_3 to C_2H_4, the corresponding ΔG for the three surfaces considered are closer; that is, neutral on Pd(111) and Pd_{55} but slightly exothermic on Pd(211) (-0.22 eV), though corresponding barriers are essentially the same as the first hydrogenation. It is clear that the first hydrogenation is decisive to the overall activity, in agreement with previous findings.[5a,b] We applied the energy span model[13] to better quantify the rate-determining states energy span (δE) and the turnover frequency (TOF) of Pd_{55}, Pd(211), and Pd(111) (Figure 1d, Figure S4, and Table S3). For Pd(111), TOF-determined intermediates (TDI) and TS (TDTS) were identified as $C_2H_2{*}+H{*}$ and TS1 with a δE of 0.96 eV, respectively. However, on both Pd_{55} and Pd(211) with TS2 identified as TDTS, stronger binding of C_2H_2 at the LCSs makes hydrogenation to C_2H_3 more endothermic with a larger δE of 1.37 and 1.29 eV, and lower TOF. This indicates that larger particles with more HCSs exposed are more active from both a kinetic and energetic point of view. H_2 dissociation on Pd(211) and Pd(111) are both facile with barriers lower than 0.22 eV at the low coverage regime (Figure S5) and are not a limiting step. Under the reaction conditions, competitive adsorption at high coverage should be considered and is examined below in detail.

Ethylene selectivity by desorption instead of further hydrogenation is investigated by difference between the hydrogenation barrier from C_2H_4 to C_2H_5 (G_{act}) and desorption barriers estimated by the absolute G_{ads} of C_2H_4; i.e., $\Delta G_s(C_2H_4)=G_{act}-|G_{ads}|$.[6d,14] A positive value implies that the C_2H_4 desorption is favorable, as found on Pd(111) with a $\Delta G_s(C_2H_4)$ of 0.14 eV, while a negative value favors further hydrogenation, as found on Pd(211) and Pd_{55} (-0.13 and -0.03 eV) (Figure 1d). To rationalize this, the C_2H_4 adsorption at the HCSs of Pd(111) (-0.78 eV) is weaker than that at the LCSs of Pd(211) and Pd_{55} (-0.93 and -0.81 eV), and C_2H_4 tends to desorb from the surfaces. Moreover, the barrier for the C_2H_4 hydrogenation on Pd(111) (0.92 eV) is higher than that of Pd(211) and Pd_{55} (0.80 and 0.78 eV) (Table S2) with favorable TSs formed at the LCSs, which indicates the larger particles would have a higher C_2H_4 selectivity. The ordering does not change at high coverages, though the coverage dependence on Pd(111) and Pd(211) are different.[5a,b] Since the C–C bond breaking was also facile at the LCSs,[15] the larger particles would alleviate the coke formation as well. Since the LCSs are undesired for the overall activity and selectivity, we focus on the HCS-rich terrace sites.

To further increase the selectivity and utilization of Pd without the expense of activity, we considered Pd overlayers on various pristine metal terraces. Specifically, we constructed epitaxial ML Pd on Rh(111), Ru(0001), and Au(111) with calculated lattice constants 2.6 %, 2.1 % smaller and 5.5 % larger than that of Pd(111), respectively. Though charge transfer between Pd and these metals is negligible (Table S4) for their close Pauling electronegativity (Ru, Rh, Pd = 2.2, Au = 2.4), there is pronounced hybridization between Pd 4*d* and Rh/Ru 4*d* or Au 5*d* (Figure 2a). Compared to the pristine Pd(111) with a surface 4*d*-band center of -1.98 eV with respect to the Fermi level, hybridization and compression downshift the d-band center to -2.40 eV for Pd/Rh(111) and -2.51 eV for Pd/Ru(0001) but upshift it to -1.63 eV for Pd/Au(111). As plotted in Figure 2b, the adsorption strength of the least saturated C_2H_2 decreases monotonically with d-band centers of 1.86, 1.75, 1.24, and 1.00 eV on Pd/Au(111), Pd(111), Pd/Rh(111), and Pd/Ru(0001), respectively, exhibiting a big change of 0.86 eV. Whereas the change becomes modest for C_2H_4 (0.39 eV), and intact for fully saturated C_2H_6 (0.04 eV).

For selectivity to ethylene, its adsorption is weakened considerably by 0.25 eV on Pd/Rh(111) and 0.39 eV on Pd/Ru(0001) compared to Pd(111). While for its hydrogenation to C_2H_5, corresponding barriers are lowered by 0.11 and 0.22 eV only (Table S2). The resulting $\Delta G_s(C_2H_4)$ increases from $+0.14$ eV for Pd(111) to $+0.28$ and $+0.31$ eV for Pd/Rh(111) and Pd/Ru(0001) (Figure 2c), respectively, and a higher selectivity to C_2H_4 is expected. For Pd/Au(111), the calculated $\Delta G_s(C_2H_4)$ is 0.20 eV, which is less selective than Pd/Rh(111) and Pd/Ru(0001).

Activity can be inferred from Figure 2d. Compared to Pd(111), the first hydrogenation becomes less endothermic by 0.20 and 0.29 eV on Pd/Rh(111) and Pd/Ru(0001), along with barriers lowered by 0.17 and 0.26 eV, but becomes more endothermic by 0.23 eV on Pd/Au(111) with a higher barrier of 0.10 eV. For the second hydrogenation, the corresponding ΔG changes from neutral to exothermic with values of -0.45 and -0.69 eV on Pd/Rh(111) and Pd/Ru(0001), with barriers lowered by 0.23 and 0.37 eV; Pd/Au(111) is endothermic with a value of 0.14 eV with no change barrier. For each hydrogenation step, the optimized TSs (Figures 2e and S3) are similar on these surfaces, and corresponding barriers decrease linearly with the forming C–H bonds of the TSs (Figure 2f). On Pd/Au(111), Pd/Rh(111), and Pd/Ru(0001), H_2 dissociation (Figure S5) is exothermic with barriers of 0.16, 0.38, and 0.52 eV, respectively, remaining lower than the hydrogenation barriers.

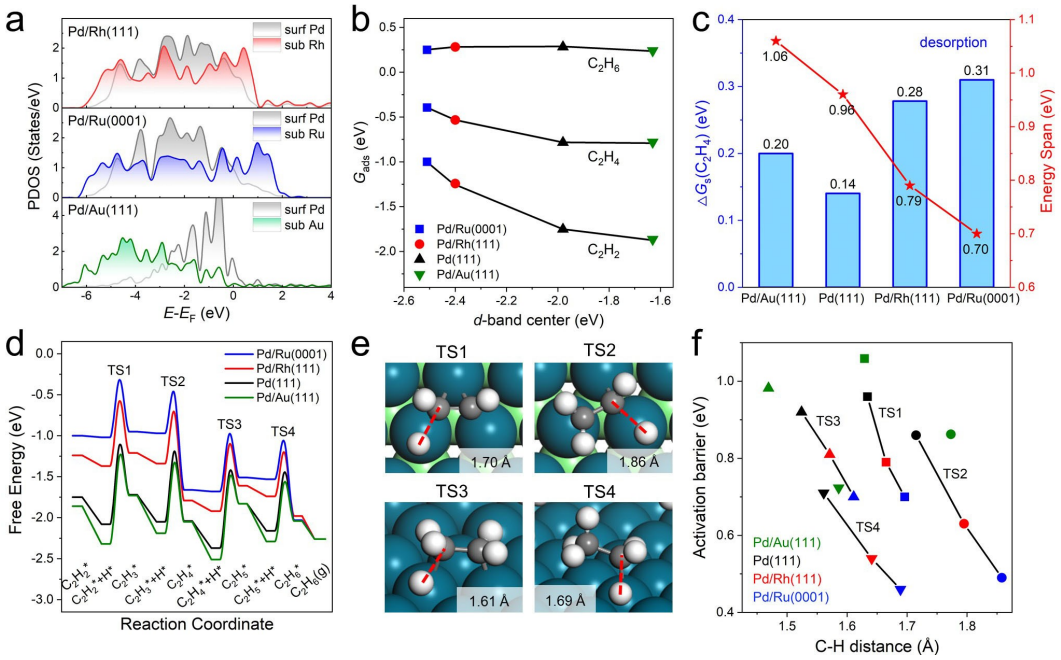

Figure 2. Calculations of Pd/Rh(111), Pd/Ru(0001), and Pd/Au(111). a) Projected density of states of *d*-band for surface Pd and subsurface Rh/Ru/Au. b) Free energies of adsorption G_{ads} for C_2H_2, C_2H_4, and C_2H_6 versus Pd 4*d* center. c) Calculated $\Delta G_s(C_2H_4)=G_{act}-|G_{ads}|$ for C_2H_4 selectivity (blue) and energy span (red) for C_2H_2 hydrogenation to C_2H_4. d) Gibbs free energy profiles of hydrogenation for C_2H_2 molecular adsorption and $2H_2$ molecular dissociative adsorption over (3×3) supercell. e) The transition states on Pd/Ru(0001) (cyan = Pd, green = Ru, gray = C, white = H). f) Barriers versus the forming C–H bond length at TSs.

Based on the energy span model (Figure 2c, Figure S4, and Table S3), Pd(111), Pd/Rh(111), Pd/Ru(0001), and Pd/Au(111) all have C_2H_2*+H* and TS1 as their TDI and TDTS, respectively. Corresponding energy spans follow the order of Pd/Au(111) (1.06 eV) > Pd(111) (0.96 eV) > Pd/Rh(111) (0.79 eV) > Pd/Ru(0001) (0.70 eV). As a result, the TOF for Pd/Ru(0001) is at least two orders of magnitude higher and much more active than the others.

To provide deep insights for improved activity on compressive Pd overlayer, we note that the adsorption of the least saturated C_2H_2 on Pd/Rh(111) and Pd/Ru(0001) is destabilized significantly by 0.51 and 0.75 eV compared to Pd(111), respectively. Whereas the destabilization for C_2H_4 becomes modest by 0.25 and 0.39 eV, and even negligible for fully saturated C_2H_6, a fact that has dramatic influences on the reactivity (Figure 3a). For C_2H_2*+2H* to C_2H_4*, the overall reaction free energy ΔG becomes more exothermic from −0.29 eV for Pd(111) to −0.55 and −0.66 eV for Pd/Rh(111) and Pd/Ru(0001), respectively. A similar trend is found for C_2H_4*+2H* to C_2H_6*, where the corresponding ΔG value changes from an endothermic value of 0.06 eV for Pd(111) to an exothermic value of −0.19 and −0.36 eV for Pd/Rh(111) and Pd/Ru(0001). Since the hydrogenation steps share similar TSs on these surfaces, a linear relationship between the energy span and reaction energies can be found (Figure 3b). For C_2H_2*+2H* to C_2H_4*, Pd/Ru(0001) has the lowest energy span of 0.70 eV for its most exothermic ΔG and therefore is the most active one. In contrast, Pd/Au(111) with a tensile strain and strong acetylene adsorption leads to an energetically unfavorable reaction and less activity even

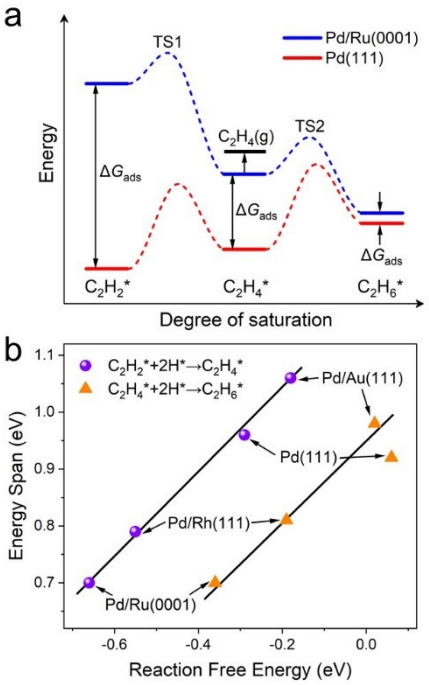

Figure 3. . a) Role of molecule saturations in semihydrogenation of acetylene on strongly bound Pd(111) and weakly bound Pd/Ru(0001) surfaces. b) Linear relationship of energy spans from C_2H_2 hydrogenation to C_2H_4 and from C_2H_4 to C_2H_6 versus reaction energies on Pd(111), Pd/Rh(111), Pd/Ru(0001), and Pd/Au(111).

than Pd(111). Here, the greatest sensitivity of the least saturated C_2H_2, as found similarly in the literature,[16] improves not only the selectivity but also the overall activity.

The Pd overlayer catalyst on Ru at the LCSs, dependence on the overlayer thickness, and stability under operando conditions were studied further. First, semihydrogenation of acetylene by Pd on well exposed Ru($10\bar{1}1$) with abundant LCSs[17] was investigated (Figure S6 and Table S2). Compared to Pd/Ru(0001), the first hydrogenation on Pd/Ru($10\bar{1}1$) becomes more endothermic by 0.49 eV along with a barrier increase of 0.15 eV, though the change in the second hydrogenation is small. The calculated G_{ads} for C_2H_4 at the LCSs is enhanced by 0.21 eV, and the corresponding $\Delta G_s(C_2H_4)$ decreases from +0.31 to +0.16 eV. This reveals that the corrugated Pd/Ru catalysts have a lower activity and selectivity to ethylene than the flat ones, but close to the pristine Pd terraces.

To see the effect of thickness of the Pd overlayers, we further investigated two ML Pd/Ru(0001) (Figure S6 and Table S2). Compared to one ML Pd/Ru(0001) above, the adsorption of C_2H_2 and C_2H_4 on a thick Pd overlayer are enhanced by 0.51 and 0.27 eV, respectively, due to the upshift of the surface Pd 4*d* center from −2.51 to −2.10 eV. Again, larger stabilization of C_2H_2 compared to C_2H_4 makes the first and second hydrogenations less energetically favorable by 0.13 and 0.53 eV, along with barriers higher by 0.21 and 0.30 eV, respectively, lowering the overall activity. The enhanced adsorption of C_2H_4 also lowers the ethylene selectivity with a decrease of $\Delta G_s(C_2H_4)$ from +0.31 to +0.21 eV. In short, one ML Pd is the optimum overlayer on Ru for semihydrogenation of acetylene.

The calculations done so far were carried out at low coverage θ, but under operando conditions θ could be considerably higher and thereby change the scenario elucidated above. To investigate this, ab initio thermodynamics[18] were used to identify the phase diagram of adsorption of the key species such as C_2H_2, C_2H_4, and H atom on Pd(111) and Pd/Ru(0001). The DFT-calculated adsorption energy (E_{ads}) per (1×1) unit cell from 1/9, 1/6, 1/4, 1/3, 1/2, 2/3, to 1 ML (Table S5) are plotted in Figure 4a. For small θ, the calculated E_{ads} is a downhill process and the corresponding adsorption is exothermic. When θ is higher than 1/3 ML, the C_2H_2 adsorption becomes uphill and endothermic, and for C_2H_4, further adsorption is too endothermic to plot in Figure 4a. Whereas for H_2 dissociative adsorption, adsorption is downhill till θ to 1 ML. We note that irrespective of the three species and the range of θ considered, the calculated E_{ads} values on Pd/Ru(0001) are always less favorable than that on Pd(111).

Based on the above energetics, the phase diagrams of adsorption of C_2H_2, C_2H_4, and H atom on Pd(111) and Pd/Ru(0001) under the operando conditions of C_2H_2 (0.01 atm), C_2H_4 (0.5 atm), and H_2 (0.02 atm) and the temperature T from 250 to 450 K are constructed and plotted in Figure 4b-d and Figure S7. On Pd(111), adsorption of 1/3 ML C_2H_2 and 1 ML H atom are the most favorable structures at the range of T considered. For C_2H_4 bound weakly to the surfaces, adsorption at 1/3 ML is dominant only when T < 341 K and becomes 1/4 ML at higher T. On Pd/Ru(0001), adsorption of 1/3 ML C_2H_2 and 1/4 ML C_2H_4 are the most

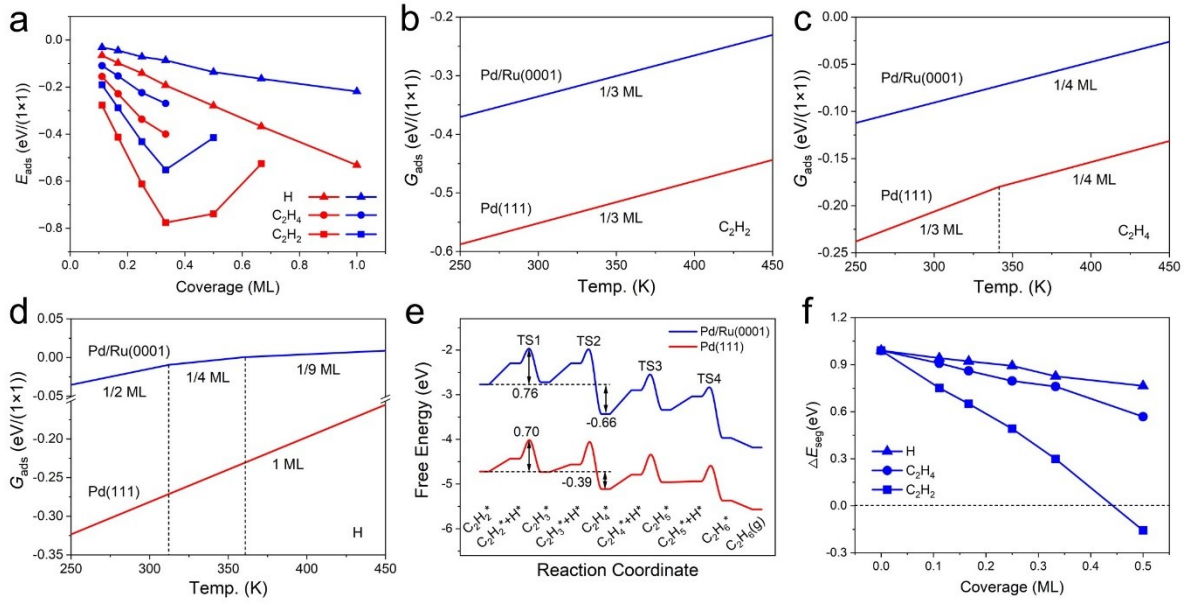

Figure 4. a) Adsorption energy per (1×1) supercell as a function of coverage for C_2H_2, C_2H_4, and dissociative atomic H on Pd(111) (red) and Pd/Ru(0001) (blue). b–d) Adsorption phase diagram in eV/(1×1) cell for C_2H_2 (0.01 atm) (b), C_2H_4 (0.5 atm) (c), and H atom (0.02 atm H_2) (d) at a wide range of temperatures on Pd(111) (red) and Pd/Ru(0001) (blue). e) Gibbs free energy profiles of hydrogenation for 3 C_2H_2 molecular adsorption and 2H_2 molecular dissociative adsorption over a (3×3) supercell. f) Calculated segregation energies in eV/(1×1) cell induced by adsorbed acetylene, ethylene, and dissociative H atom on Pd/Ru(0001).

favorable structures at the range of T considered. For H atom, 1/2 ML is preferred when $T < 312$ K, but decreases to 1/4 ML at higher T, and 1/9 ML when $T > 360$ K. Compared to C_2H_4 and H_2 dissociative adsorption (Figure 4b–d), adsorption of C_2H_2 is more exothermic and therefore is the dominating species under the operando conditions, irrespective of Pd(111) and Pd/Ru(0001).

We investigated the semihydrogenation on Pd(111) and Pd/Ru(0001) with pre-adsorbed 1/3 ML C_2H_2 in a (3×3) supercell, and the resulting free energy profiles are shown in Figure 4e (key structures in Figure S8). For hydrogenation of C_2H_2* to C_2H_4*, the overall free energy on Pd(111) is exothermic of −0.39 eV, but becomes more exothermic of −0.66 eV on Pd/Ru(0001). Kinetically, as indicated in Figure 4e, the corresponding apparent barriers of 0.70 and 0.76 eV are however very close. These together indicate that for the first two hydrogenations, Pd/Ru(0001) remains more active than Pd(111) even under operando conditions. We note that with pre-adsorbed 1/3 ML C_2H_2*, H_2 dissociative adsorption becomes endothermic on both surfaces, contributing significantly to the apparent barriers. Accordingly, the saturated H coverage is low. This is different from the low θ, where the apparent barriers are decided by hydrogenations (Figure 2d). For selectivity, calculated $\Delta G_s(C_2H_4)$ on Pd(111) becomes negative (−0.10 eV), implying hydrogenation to ethane is preferential, in contrast to the positive value of 0.14 eV at the low θ. Nevertheless, $\Delta G_s(C_2H_4)$ on Pd/Ru(0001) is still positive (+0.09 eV), and high ethylene selectivity is retained.

Pd overlayers on Ru might be unstable and segregate under operando conditions due to stronger adsorption of reactants on Ru compared to Pd.[19] We calculated the segregation cost ΔE_{seg} between the Pd atom in the overlayer and subsurface Ru atom. In the absence of the adsorbates, the calculated ΔE_{seg} is endothermic of ca. 0.99 eV/Pd atom (Figure S9). For segregation into the bulk, it increases to 1.16 eV/Pd atom (Figure S10), in good agreement with the literature value of 1.03 eV,[20] and 0.84 eV for Pd in a 55-atom Pd@Ru alloy cluster.[21] To investigate the adsorbate-induced segregation, C_2H_2, C_2H_4, and H atom at 1/9, 1/6, 1/4, 1/3, and 1/2 ML were considered, and the calculated ΔE_{seg} are plotted in Figure 4f. For adsorbed C_2H_4 and dissociative H atoms, the endothermic ΔE_{seg} in the range of θ considered implies that their presence cannot change the Pd/Ru(0001) structure. C_2H_2 might induce Ru segregation (exothermic ΔE_{seg}) only if $\theta \geq 1/2$ ML, but the above phase diagrams reveal that the corresponding saturation coverage is 1/3 ML only. Namely, Pd/Ru(0001) is stable under the reaction conditions of semihydrogenation of acetylene.

Based on the above calculations, we first synthesized two Pd/SiO_2 catalysts with Pd particle sizes of 1.6 ± 0.6 and 5.1 ± 0.5 nm using the wet impregnation (WI) method (denoted as Pd(1.6 nm)/SiO_2 and Pd(5.1 nm)/SiO_2, Figure S11a,b), to understand the Pd particle size effect with different distributions in LCSs and HCSs for semihydrogenation of acetylene. Next, we also synthesized SiO_2-supported Ru@Pd core–shell catalysts with different Pd coverages. Therein, Ru NPs with a size of 5.1 ± 0.5 nm and a loading of 4 wt.% on SiO_2 (denoted as Ru(5.1 nm)/SiO_2, Figure S11c) were first prepared using the WI method and confirmed by inductively coupled plasma atomic emission spectroscopy (ICP-AES). After that, Pd was selectively deposited onto Ru particles but not on the SiO_2 support using ALD at 150 °C, a technique that relies on sequential molecular-level surface reactions (Figure 5a).[22] The selective deposition was verified by ICP-AES analysis of the Pd contents after Pd deposition on Ru/SiO_2 and blank SiO_2 (Figure S12). After performing 3, 5, and 7 cycles of Pd ALD on Ru(5.1 nm)/SiO_2, the Pd loadings were 0.40, 0.91, and 1.38 wt.%, respectively, estimated to be 0.7, 1.6, and 2.3 Pd MLs according to the cuboctahedron cluster model with a cubic close-packed structure[23] and therefore denoted as Ru(5.1 nm)@0.7ML-Pd, Ru(5.1 nm)@1.6ML-Pd, and Ru(5.1 nm)@2.3ML-Pd. Transmission electron microscopy (TEM) showed that the particle size grew to about 5.3 ± 1.0, 5.8 ± 0.6, and 6.1 ± 0.6 nm after 3, 5, and 7 cycles of Pd ALD, respectively (Figure 5b–d), with indications of a Pd shell growth rate of ca. 0.8 Å per ALD cycle, in line with our previous work.[24] Elemental mapping using energy dispersive X-ray spectroscopy (EDS) verified the selective deposition of Pd, and the formation of the Ru@Pd core–shell structure (Figure 5e–h). X-ray diffraction measurements also showed that the locations of the Ru diffraction peaks persisted without any shift (Figure S13), further supporting the formation of the Ru@Pd core–shell structure.

Figure 6a shows a representative aberration-corrected high-angle annular dark field scanning TEM (HAADF-STEM) image of a Ru(5.1 nm)@0.7ML-Pd bimetallic NP. Though Ru and Pd have hardly any contrast in brightness due to their close atomic numbers, line intensity profiles (Figure 6b) revealed that the interlayer distance between the outer most layer and the second layer was about 0.230 nm, enlarged substantially relative to that of the bulk (ca. 0.217 nm), indicating the presence of a Pd shell with a larger atomic size. It is evidenced that the Pd overlayer on Ru NPs has a thickness of 1 to 2 atomic layers, which is consistent with the particle size statistics in the insets of Figure 5b–d. Diffuse reflectance infrared Fourier transform spectroscopy (DRIFTS) of CO chemisorption showed that Ru(5.1 nm)/SiO_2 exhibited three vibrational peaks at 2127.4, 2069.0, and 2040.2 cm^{-1}, assigned to Ru^{n+}-$(CO)_3$, Ru^{n+}-(CO), and Ru-CO, respectively (Figure 6c).[25] After Pd ALD on Ru(5.1 nm)/SiO_2, a new peak at ca. 1990 cm^{-1} appeared and was assigned to bridge-bonded CO on Pd, confirming again the nucleation of Pd on Ru. The intensity of this peak increased with the Pd ALD cycles, indicating sequential deposition of Pd on Ru NPs with 1 to 2 atomic layers of thickness. We can observe that the two peaks attributed to CO adsorption on Ru (around 2135 and 2078 cm^{-1}) were preserved after Pd ALD even for 7 cycles, indicating that Ru was not fully covered by Pd in all Ru@Pd samples synthesized by formation of the Ru core-Pd rich shell structure.

The catalytic performance of Pd/SiO_2 and $Pd@Ru/SiO_2$ samples in semihydrogenation of acetylene in excess ethylene was evaluated in a fixed-bed reactor under ambient pressure with a hydrogen to acetylene ratio of 2:1. Pd(1.6 nm)/SiO_2 showed complete conversion of C_2H_2 at

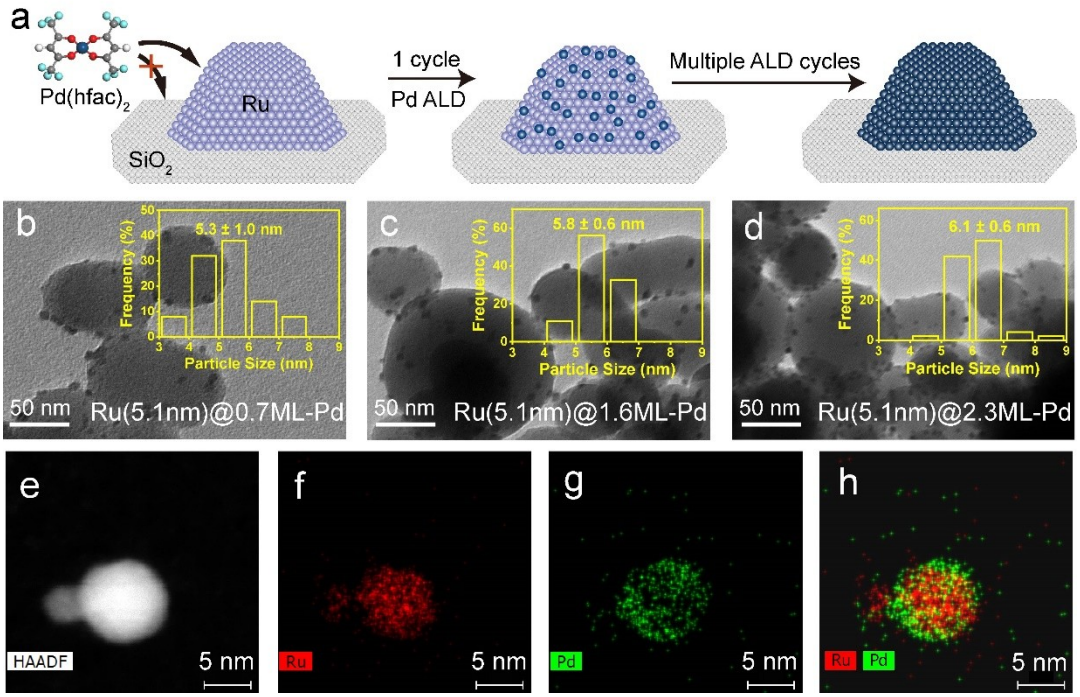

Figure 5. Synthesis and morphology of Ru@Pd catalysts. a) Illustration of the synthesis of Ru@Pd bimetallic catalysts using selective Pd ALD. TEM images of b) Ru(5.1 nm)@0.7ML-Pd, c) Ru(5.1 nm)@1.6ML-Pd, d) Ru(5.1 nm)@2.3ML-Pd. The insets are the corresponding NPs size distribution. e) STEM image of Ru(5.1 nm)@2.3 ML-Pd and the corresponding EDS elemental mapping signals: f) Ru Lα, g) Pd Lα, and the constructed h) Ru + Pd.

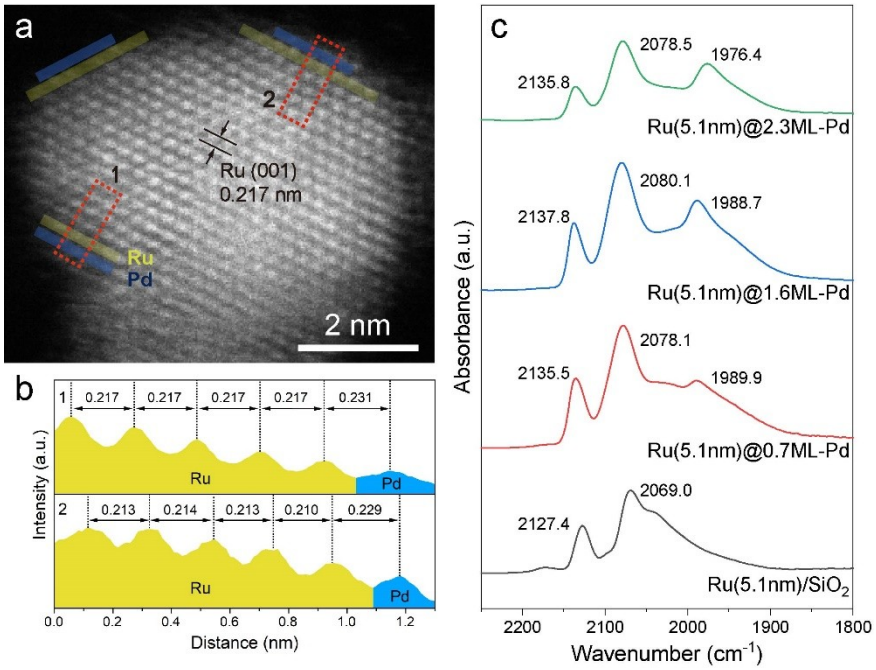

Figure 6. a) A representative atomic-resolution HAADF-STEM image of Ru(5.1 nm)@0.7ML-Pd, along with b) the corresponding line intensity profiles along the numbered dashed rectangles to show the distance of the interplanar distance. c) DRIFTS CO chemisorption of the Ru@Pd samples with different Pd coverages at the CO saturation coverage.

102 °C, whereas Pd(5.1 nm)/SiO_2 achieved complete conversion at a much lower temperature of 48 °C (Figure 7a). The mass specific activity based on the Pd content at 40 °C was 14.5 and 50.7 $g_{C2H2}\,g_{Pd}^{-1}\,h^{-1}$ for Pd(1.6 nm)/SiO_2 and Pd-

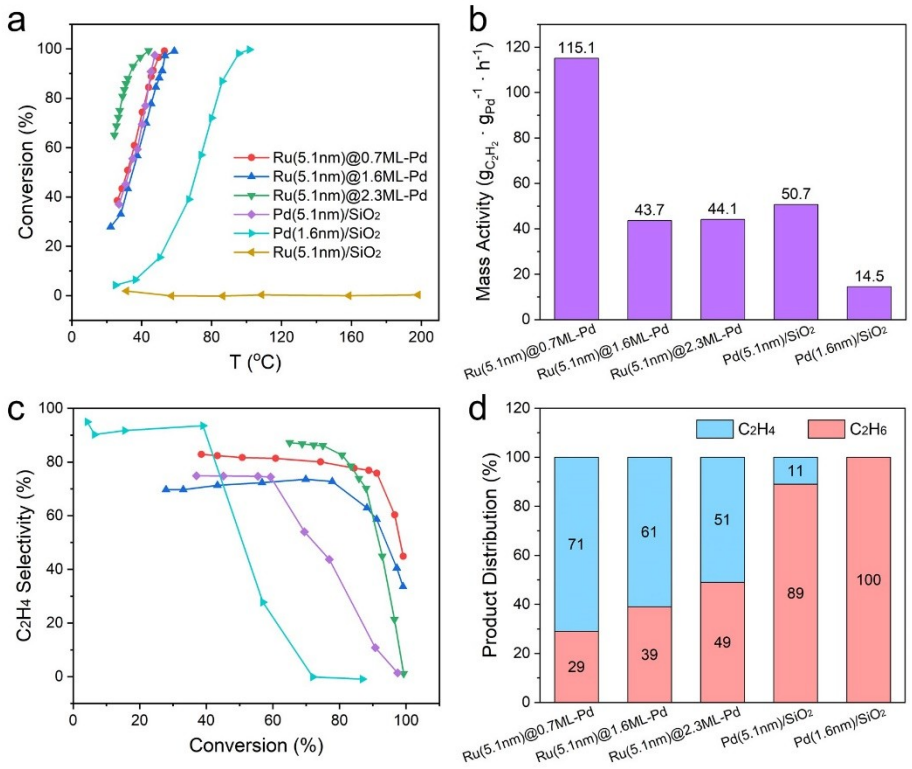

Figure 7. The catalytic performances of different catalysts in semihydrogenation of acetylene in excess of ethylene. a) Acetylene conversion as a function of the reaction temperatures. The amount of catalysts used are controlled to be 20 mg for each sample. b) Mass activity at the reaction temperature of 40 °C. c) C_2H_4 selectivity as a function of corresponding conversion. The legends in a) also apply to c). d) The products distribution at 90 % C_2H_2 conversion in the semihydrogenation of C_2H_2 in the presence of excess ethylene.

(5.1 nm)/SiO_2, respectively (Figure 7b). At 90 % C_2H_2 conversion, Pd(1.6 nm)/SiO_2 with a smaller Pd size showed zero C_2H_4 selectivity, whereas Pd(5.1 nm)/SiO_2 had a higher C_2H_4 selectivity of 11 % (Figure 7c,d). Higher activity and selectivity to ethylene for the large Pd particles exposing more HCSs are in good agreement with theoretical calculations (Figure 1), and also consistent with the previous work.[26] For instance, Borodziński et al. found that the TOF of Pd/SiO_2 in the steady state increased from about 0.3 to 1.7 $p_{H2}^{-1} s^{-1} kPa^{-1}$ with the particle size from 4.2 to 26.2 nm.[27]

As shown in Figure 7a, all the Ru@Pd catalysts prepared achieved complete conversion of acetylene at ca. 50 °C, manifesting their high activity. Calculation of the mass activity based on the Pd content revealed that Ru(5.1 nm)-@0.7ML-Pd showed the highest mass activity, reaching 115.1 $g_{C2H2}\, g_{Pd}^{-1} h^{-1}$ at 40 °C, which is more than 2 times higher than Pd(5.1 nm)/SiO_2 and 8 times higher than Pd-(1.6 nm)/SiO_2 (Figure 7b and Table S6). Whereas for Ru-(5.1 nm)@1.6ML-Pd and Ru(5.1 nm)@2.3ML-Pd, the corresponding mass specific activity decreases significantly and becomes comparable to Pd(5.1 nm)/SiO_2. The ethylene selectivity reached as high as 71 %, 61 %, and 51 % at 90 % conversion on Ru(5.1 nm)@0.7ML-Pd, Ru(5.1 nm)@1.6ML-Pd, and Ru(5.1 nm)@2.3ML-Pd (Figure 7c,d), respectively, which is considerably higher than Pd(5.1 nm)/SiO_2 (11 %) and the previous results.[28] These experimental results show that Ru(5.1 nm)@0.7ML-Pd exhibits remarkably high activity and much enhanced selectivity at high conversion compared to Pd(5.1 nm)/SiO_2, substantiating the theoretical predictions. Moreover, increasing the thickness of the Pd shell by more than 1 ML lowers the corresponding activity and selectivity, in good agreement with trend behaviors revealed from the calculations. Additionally, Ru@Pd catalysts showed comparable stability with Pd under long-term operation of 19 hours (Figure S14), also corroborating the stability against segregation found by the calculations. We note that ternary Al–Pd–Ru cubic crystalline icosahedral approximants demonstrated high activity and selectivity for acetylene semihydrogenation.[29]

In contrast to the highly efficient bimetallic core–shell Ru@Pd catalysts, Ru(5.1 nm)/SiO_2 did not show any activity up to 200 °C. We did not observe color change for the used Ru catalysts, accordingly, coke formation for the inactivity is excluded. Zero conversion might arise from C_2H_2 poisoning due to its too strong binding (−2.59 eV) on Ru(0001), even stronger than that of Pd(111) (Table S1). Based on the endothermic dissociative adsorption of H_2 on Pd(111) with preadsorbed 1/3 ML C_2H_2, more severe site blockage and hindrance to H_2 activation is expected on Ru(0001) covered with more C_2H_2. The present work is in agreement with the low activity of pure Ru catalysts observed in the literature.[30]

Conclusion

Based on comprehensive DFT and ab initio thermodynamics investigations, the least saturated molecule is revealed as the most structurally sensitive compared to the more saturated molecules—a fact that is utilized to simultaneously boost the activity and selectivity of semihydrogenation of acetylene to ethylene by Pd-based catalysts. Compared to the HCSs, the larger stabilization of the least saturated acetylene compared to the more saturated ethylene at the LCSs makes the hydrogenation of acetylene to ethylene less favorable, and yet the stabilized ethylene is reluctant to desorb. Accordingly, a decrease of the Pd particle sizes cannot improve the activity without a detrimental effect on the ethylene selectivity, as supported by experiments. Simultaneous promotion of both activity and selectivity is predicted by fabricating Ru terrace supported Pd ML in compression, which is resistant to segregation under reaction conditions. The larger destabilization of acetylene compared to that of ethylene makes the acetylene hydrogenation to ethylene more exothermic to boost the activity, and the destabilized ethylene is favorable for facile desorption and high ethylene selectivity. These predictions were used to guide the experiments, whereby large size Ru@Pd core–shell catalysts with ML thickness were synthesized using ALD, exhibiting high ethylene selectivity at high conversion and high activity, superior to the Ru@Pd core–shell catalysts with a thicker shell and monometallic Pd nanocatalysts.

Acknowledgements

This work was supported by the National Key R&D Program of China (2018YFA0208603, 2021YFA1502802), the National Natural Science Foundation of China (22221003, 91945302, 22025205), K. C. Wong Education (GJTD-2020-15), and the Fundamental Research Funds for the Central Universities (20720220009, WK2060000038). The authors also gratefully thank the Supercomputing Center of University of Science and Technology of China.

Conflict of Interest

The authors declare no conflict of interest.

Data Availability Statement

The data that support the findings of this study are available from the corresponding author upon reasonable request.

Keywords: Atomic Layer Deposition · First-Principles Calculations · Molecule Saturation · Semihydrogenation of Acetylene · Strained Bimetallic Overlayer

[1] a) S. Dahl, A. Logadottir, C. J. H. Jacobsen, J. K. Nørskov, *Appl. Catal. A* **2001**, *222*, 19–29; b) T. Bligaard, J. K. Nørskov, S. Dahl, J. Matthiesen, C. H. Christensen, J. Sehested, *J. Catal.* **2004**, *224*, 206–217; c) A. J. Medford, A. Vojvodic, J. S. Hummelshøj, J. Voss, F. Abild-Pedersen, F. Studt, T. Bligaard, A. Nilsson, J. K. Nørskov, *J. Catal.* **2015**, *328*, 36–42.

[2] a) M. Jørgensen, H. Grönbeck, *J. Am. Chem. Soc.* **2019**, *141*, 8541–8549; b) H. Wang, X.-K. Gu, X. Zheng, H. Pan, J. Zhu, S. Chen, L. Cao, W.-X. Li, J. Lu, *Sci. Adv.* **2019**, *5*, eaat6413; c) Q. Guan, C. Zhu, Y. Lin, E. I. Vovk, X. Zhou, Y. Yang, H. Yu, L. Cao, H. Wang, X. Zhang, X. Liu, M. Zhang, S. Wei, W.-X. Li, J. Lu, *Nat. Catal.* **2021**, *4*, 840–849.

[3] a) G. S. Parkinson, Z. Novotny, G. Argentero, M. Schmid, J. Pavelec, R. Kosak, P. Blaha, U. Diebold, *Nat. Mater.* **2013**, *12*, 724–728; b) S. Duan, R. Wang, J. Liu, *Nanotechnology* **2018**, *29*, 204002; c) A. Wang, J. Li, T. Zhang, *Nat. Chem. Rev.* **2018**, *2*, 65–81; d) S. Hu, W.-X. Li, *Science* **2021**, *374*, 1360–1365.

[4] a) A. Borodzinki, *Catal. Rev. Sci. Eng.* **2006**, *48*, 91–144; b) A. Borodzinski, G. C. Bond, *Catal. Rev. Sci. Eng.* **2008**, *50*, 379–469; c) T. Ren, M. Patel, K. Blok, *Energy* **2008**, *33*, 817–833; d) Y. Gao, L. Neal, D. Ding, W. Wu, C. Baroi, A. M. Gaffney, F. Li, *ACS Catal.* **2019**, *9*, 8592–8621.

[5] a) W. Xie, P. Hu, *Catal. Sci. Technol.* **2021**, *11*, 5212–5222; b) W. Xie, J. Xu, Y. Ding, P. Hu, *ACS Catal.* **2021**, *11*, 4094–4106; c) I. Y. Ahn, J. H. Lee, S. K. Kim, S. H. Moon, *Appl. Catal. A* **2009**, *360*, 38–42; d) D. V. Glyzdova, T. N. Afonasenko, E. V. Khramov, N. N. Leont'eva, I. P. Prosvirin, A. V. Bukhtiyarov, D. A. Shlyapin, *Appl. Catal. A* **2020**, *600*, 117627; e) Y. Niu, X. Huang, Y. Wang, M. Xu, J. Chen, S. Xu, M.-G. Willinger, W. Zhang, M. Wei, B. Zhang, *Nat. Commun.* **2020**, *11*, 3324.

[6] a) L. Chen, X.-T. Li, S. Ma, Y.-F. Hu, C. Shang, Z.-P. Liu, *ACS Catal.* **2022**, *12*, 14872–14881; b) X.-T. Li, L. Chen, C. Shang, Z. P. Liu, *J. Am. Chem. Soc.* **2021**, *143*, 6281–6292; c) H. Zhou, X. Yang, L. Li, X. Liu, Y. Huang, X. Pan, A. Wang, J. Li, T. Zhang, *ACS Catal.* **2016**, *6*, 1054–1061; d) Q. Feng, S. Zhao, Y. Wang, J. Dong, W. Chen, D. He, D. Wang, J. Yang, Y. Zhu, H. Zhu, L. Gu, Z. Li, Y. Liu, R. Yu, J. Li, Y. Li, *J. Am. Chem. Soc.* **2017**, *139*, 7294–7301; e) Y. Cao, H. Zhang, S. Ji, Z. Sui, Z. Jiang, D. Wang, F. Zaera, X. Zhou, X. Duan, Y. Li, *Angew. Chem. Int. Ed.* **2020**, *59*, 11647–11652; f) X. Ge, Y. Cao, K. Yan, Y. Li, L. Zhou, S. Dai, J. Zhang, X. Gong, G. Qian, X. Zhou, W. Yuan, X. Duan, *Angew. Chem. Int. Ed.* **2022**, *61*, e202215225; g) F. Studt, F. Abild-Pedersen, T. Bligaard, R. Z. Sorensen, C. H. Christensen, J. K. Nørskov, *Science* **2008**, *320*, 1320–1322.

[7] a) F. Huang, Y. Deng, Y. Chen, X. Cai, M. Peng, Z. Jia, P. Ren, D. Xiao, X. Wen, N. Wang, H. Liu, D. Ma, *J. Am. Chem. Soc.* **2018**, *140*, 13142–13146; b) C. Riley, S. Zhou, D. Kunwar, A. De La Riva, E. Peterson, R. Payne, L. Gao, S. Lin, H. Guo, A. Datye, *J. Am. Chem. Soc.* **2018**, *140*, 12964–12973; c) S. Wei, A. Li, J.-C. Liu, Z. Li, W. Chen, Y. Gong, Q. Zhang, W. C. Cheong, Y. Wang, L. Zheng, H. Xiao, C. Chen, D. Wang, Q. Peng, L. Gu, X. Han, J. Li, Y. Li, *Nat. Nanotechnol.* **2018**, *13*, 856–861; d) R. Gao, J. Xu, J. Wang, J. Lim, C. Peng, L. Pan, X. Zhang, H. Yang, J.-J. Zou, *J. Am. Chem. Soc.* **2022**, *144*, 573–581; e) F. Huang, M. Peng, Y. Chen, X. Cai, X. Qin, N. Wang, D. Xiao, L. Jin, G. Wang, X. D. Wen, H. Liu, D. Ma, *J. Am. Chem. Soc.* **2022**, *144*, 18485–18493; f) F. Huang, Y. Deng, Y. Chen, X. Cai, M. Peng, Z. Jia, J. Xie, D. Xiao, X. Wen, N. Wang, Z. Jiang, H. Liu, D. Ma, *Nat. Commun.* **2019**, *10*, 4431.

[8] a) G. X. Pei, X. Y. Liu, A. Wang, A. F. Lee, M. A. Isaacs, L. Li, X. Pan, X. Yang, X. Wang, Z. Tai, K. Wilson, T. Zhang, *ACS Catal.* **2015**, *5*, 3717–3725; b) H. Yan, H. Cheng, H. Yi, Y. Lin, T. Yao, C. Wang, J. Li, S. Wei, J. Lu, *J. Am. Chem. Soc.* **2015**, *137*, 10484–10487; c) M. Yang, L. F. Allard, M. Flytzani-Stephanopoulos, *J. Am. Chem. Soc.* **2013**, *135*, 3768–3771; d) S. Horch, H. T. Lorensen, S. Helveg, E. Lægsgaard, I. Stensgaard, K. W. Jacobsen, J. K. Nørskov, F. Besenbacher, *Nature* **1999**,

398, 134–136; e) D. Yang, P. Xu, N. D. Browning, B. C. Gates, *J. Phys. Chem. Lett.* **2016**, *7*, 2537–2543.
[9] a) S. Alayoglu, A. U. Nilekar, M. Mavrikakis, B. Eichhorn, *Nat. Mater.* **2008**, *7*, 333–338; b) A. U. Nilekar, S. Alayoglu, B. Eichhorn, M. Mavrikakis, *J. Am. Chem. Soc.* **2010**, *132*, 7418–7428; c) S. Alayoglu, B. Eichhorn, *J. Am. Chem. Soc.* **2008**, *130*, 17479–17486; d) K. Kim, J. Byun, H. Kim, K.-S. Lee, H. S. Lee, J. Kim, T. Hyeon, J. J. Kim, J. W. Han, *ACS Catal.* **2021**, *11*, 15089–15097.
[10] J. E. S. van der Hoeven, J. Jelic, L. A. Olthof, G. Totarella, R. J. A. van Dijk-Moes, J.-M. Krafft, C. Louis, F. Studt, A. van Blaaderen, P. E. de Jongh, *Nat. Mater.* **2021**, *20*, 1216–1220.
[11] D. Gao, H. Zhou, J. Wang, S. Miao, F. Yang, G. Wang, J. Wang, X. Bao, *J. Am. Chem. Soc.* **2015**, *137*, 4288–4291.
[12] J. Horiuti, M. Polanyi, *Nature* **1934**, *134*, 377–378.
[13] a) S. Kozuch, S. Shaik, *Acc. Chem. Res.* **2011**, *44*, 101–110; b) S. Kozuch, J. M. L. Martin, *ChemPhysChem* **2011**, *12*, 1413–1418; c) S. Kozuch, *ACS Catal.* **2015**, *5*, 5242–5255; d) E. Solel, N. Tarannam, S. Kozuch, *Chem. Commun.* **2019**, *55*, 5306–5322.
[14] a) B. Yang, R. Burch, C. Hardacre, G. Headdock, P. Hu, *ACS Catal.* **2012**, *2*, 1027–1032; b) B. Yang, R. Burch, C. Hardacre, G. Headdock, P. Hu, *J. Catal.* **2013**, *305*, 264–276.
[15] J. Lu, B. Fu, M. C. Kung, G. Xiao, J. W. Elam, H. H. Kung, P. C. Stair, *Science* **2012**, *335*, 1205–1208.
[16] a) F. Abild-Pedersen, J. Greeley, F. Studt, J. Rossmeisl, T. R. Munter, P. G. Moses, E. Skulason, T. Bligaard, J. K. Nørskov, *Phys. Rev. Lett.* **2007**, *99*, 016105; b) G. Jones, F. Studt, F. Abild-Pedersen, J. K. Nørskov, T. Bligaard, *Chem. Eng. Sci.* **2011**, *66*, 6318–6323.
[17] a) W.-Z. Li, J.-X. Liu, J. Gu, W. Zhou, S.-Y. Yao, R. Si, Y. Guo, H.-Y. Su, C.-H. Yan, W.-X. Li, Y.-W. Zhang, D. Ma, *J. Am. Chem. Soc.* **2017**, *139*, 2267–2276; b) H. Lin, J.-x. Liu, H.-j. Fan, W.-x. Li, *Chin. J. Chem. Phys.* **2021**, *34*, 263–272; c) A. Ishikawa, T. Doi, H. Nakai, *J. Catal.* **2018**, *357*, 213–222.
[18] a) K. Reuter, M. Scheffler, *Phys. Rev. B* **2001**, *65*, 035406; b) W.-X. Li, C. Stampfl, M. Scheffler, *Phys. Rev. Lett.* **2003**, *90*, 256102.
[19] a) F. Tao, M. E. Grass, Y. Zhang, D. R. Butcher, J. R. Renzas, Z. Liu, J. Y. Chung, B. S. Mun, M. Salmeron, G. A. Somorjai, *Science* **2008**, *322*, 932–934; b) K. J. Andersson, F. Calle-Vallejo, J. Rossmeisl, I. Chorkendorff, *J. Am. Chem. Soc.* **2009**, *131*, 2404–2407; c) A. J. Logsdail, L. O. Paz-Bórbon, C. A. Downing, *J. Phys. Chem. C* **2018**, *122*, 5721–5730; d) J. S. Lim, J. Vandermause, M. A. van Spronsen, A. Musaelian, Y. Xie, L. Sun, C. R. O'Connor, T. Egle, N. Molinari, J. Florian, K. Duanmu, R. J. Madix, P. Sautet, C. M. Friend, B. Kozinsky, *J. Am. Chem. Soc.* **2020**, *142*, 15907–15916; e) J. Greeley, M. Mavrikakis, *Nat. Mater.* **2004**, *3*, 810–815; f) J. Greeley, M. Mavrikakis, *Catal. Today* **2006**, *111*, 52–58.
[20] A. V. Ruban, H. L. Skriver, J. K. Nørskov, *Phys. Rev. B* **1999**, *59*, 15990–16000.
[21] L.-L. Wang, D. D. Johnson, *J. Am. Chem. Soc.* **2009**, *131*, 14023–14029.
[22] a) J. Lu, K.-B. Low, Y. Lei, J. A. Libera, A. Nicholls, P. C. Stair, J. W. Elam, *Nat. Commun.* **2014**, *5*, 3264; b) J. Lu, J. W. Elam, P. C. Stair, *Surf. Sci. Rep.* **2016**, *71*, 410–472.
[23] J. He, I. Ichinose, T. Kunitake, A. Nakao, Y. Shiraishi, N. Toshima, *J. Am. Chem. Soc.* **2003**, *125*, 11034–11040.
[24] H. Wang, C. Wang, H. Yan, H. Yi, J. Lu, *J. Catal.* **2015**, *324*, 59–68.
[25] M. Kantcheva, S. Sayan, *Catal. Lett.* **1999**, *60*, 27–38.
[26] a) C. Gigola, H. Aduriz, P. Bodnariuk, *Appl. Catal.* **1986**, *27*, 133–144; b) H. Adúriz, P. Bodnariuk, M. Dennehy, C. Gigola, *Appl. Catal.* **1990**, *58*, 227–239; c) M. Ruta, N. Semagina, L. Kiwi-Minsker, *J. Phys. Chem. C* **2008**, *112*, 13635–13641.
[27] a) A. Borodziński, *Catal. Lett.* **2001**, *71*, 169–175; b) A. Borodziński, A. Cybulski, *Appl. Catal. A* **2000**, *198*, 51–66.
[28] a) S. Leviness, V. Nair, A. H. Weiss, Z. Schay, L. Guczi, *J. Mol. Catal.* **1984**, *25*, 131–140; b) Q. Zhang, J. Li, X. Liu, Q. Zhu, *Appl. Catal. A* **2000**, *197*, 221–228; c) W.-J. Kim, S. H. Moon, *Catal. Today* **2012**, *185*, 2–16.
[29] K. Abe, R. Tsukuda, N. Fujita, S. Kameoka, *RSC Adv.* **2021**, *11*, 15296–15300.
[30] C. J. Heard, C. Hu, M. Skoglundh, D. Creaser, H. Grönbeck, *ACS Catal.* **2016**, *6*, 3277–3286.

Manuscript received: January 3, 2023
Accepted manuscript online: April 7, 2023
Version of record online: April 28, 2023